Int. J. Heat Mass Transfer. Vol. 36, No. 6, pp. 1529–1539, 1993
Printed in Great Britain

0017-9310/93 $6.00 + 0.00

Natural convection in an annular fluid layer rotating at weak angular velocity

M. PRUD'HOMME, L. ROBILLARD and M. HILAL
Département de Génie Mécanique, École Polytechnique de Montréal, C.P.6079 A, Montréal H3C 3A7, Québec, Canada

(*Received* 4 *March* 1992 *and in final form* 7 *July* 1992)

Abstract—A study is made of natural convection in an annular fluid layer confined between two horizontal cylindrical boundaries rotating at the same angular velocity. The problem is solved for two-dimensional flow with isothermal boundaries, the outer boundary being warmer, using perturbation and numerical methods. The weak rotation regime only is considered, for which centrifugal acceleration is neglected. Governing equations for the flow field are solved in a non-inertial coordinate system rotating with the boundaries, in order to remove uniform, solid-body rotation effects from the pure natural convection flow. Results reveal that a significant mass of fluid far from the boundaries remains tied up to the gravity vector at first, when the angular velocity is small, and thus does not take part in the solid-body rotation. This creates a net circulating flow around the annulus in the rotating system, the intensity of which is shown analytically to be proportional to $Ra^2 Re$ for incipient convection. Perturbation solutions are in good agreement with numerical data for Rayleigh numbers up to several hundreds, depending on the radius ratio. At high Rayleigh numbers, a bifurcation exists between the circulating and solid-body rotation flow regimes, in contrast with the smooth transition observed at lower Rayleigh numbers. Hysteresis effects are observed over a certain range of Reynolds numbers, provided that the Rayleigh number is high enough.

1. INTRODUCTION

THE GENERAL problem of natural convection in rotating systems has been the subject of a great deal of investigations so far. While rotation about a vertical axis has been studied intensively, since this configuration is frequently encountered in engineering problems, comparatively little work has ever been done on low-speed rotation about an horizontal axis, which is also of practical importance. The relevant fields of application include crystal growth [1] and the processing of canned liquids [2, 3], among others. In the latter case, the processing often involves some form of thermal treatment while the can is rotating. The heat transfer rates can be significantly affected by the flow established within the liquid under the combined influences of rotation and buoyancy.

Free convection between two horizontal isothermal cylinders, with the stationary outer cylinder and the inner cylinder rotating about its axis at constant angular velocity, was considered by Lee [4] and Fusegi *et al.* [5]. The analysis was restricted in both cases to the cross-sectional plane and did not allow for the three-dimensional effects resulting from the appearance of Taylor vortices. In this respect, the authors purposedly limited their numerical calculations to a range of parameters that would exclude this possibility from the start. Lee treated the problem over a good range of Rayleigh numbers, allowing for both horizontal and vertical eccentricities of the inner cylinder. It was concluded that the mean Nusselt number increases with the Rayleigh number at a given angular velocity, and decreases with the rotation speed, all the other parameters being kept constant. Fusegi *et al.* did not consider the eccentric case but treated the problem for both high and low values of the densimetric Froude number σ (which expresses the relative magnitude of buoyancy versus rotation effects), whereas Lee had focused mainly on the low σ results. Using an unusual velocity–vorticity formulation, which proved to be very stable numerically, they reached similar conclusions.

Yang *et al.* [1] studied natural convection inside a single horizontal rotating cylinder, with both ends maintained at different temperatures. In that case, the pure conduction heat transfer is present in the horizontal direction. They formulated the problem in both inertial and non-inertial frames and found a steady-state flow regime in the inertial frame. According to their results, free convection affects the heat transfer rates mainly at low rotation speeds. Increasing the rotation speed resulted in almost a solid-body rotation flow for which heat transfer rates returned to their pure conduction levels. The effects of rotation on an annular saturated porous layer were investigated recently by Robillard and Torrance [6]. A net circulating flow around the annulus relative to the solid matrix was detected and the convective heat transfer was found to decrease monotonically to zero with increasing rotation speed. Subsequently, Ladeinde and Torrance [7] treated the case of a rotating horizontal cylinder with constant volumetric heating and fixed wall temperature, using a finite element solution procedure. Unlike all the studies quoted above, they did not make the weak rotation approximation which drops radial acceleration in the Boussinesq term, but

NOMENCLATURE

g	gravity [m s^{-2}]
$\hat{\mathbf{g}}$	unit vector along gravity
J	Bessel function of the first kind
K	modified Bessel function of the second kind
Nu	average Nusselt number
p	pressure [Pa]
Pr	Prandtl number, ν/α
r	radial coordinate [m]
R	aspect ratio, r_2/r_1
Re	Reynolds number, $\Omega r_1^2/\nu$
Ra	Rayleigh number, $\beta(T_2-T_1)r_1^3 g/\nu\alpha$
t	time [s]
T	temperature [C]
$\mathbf{u}$	velocity vector, (u, v) [m s^{-1}]
$\hat{\mathbf{z}}$	unit vector normal to the r, θ plane.

Greek symbols

α	thermal diffusivity [m^2 s^{-1}]
β	thermal expansion coefficient [K^{-1}]
θ	angular coordinate
ν	kinematic viscosity [m^2 s^{-1}]
ρ	density [kg m^{-3}]
σ	densimetric Froude number, $Ra/Re^2 Pr$
τ	net shear torque
φ	parameter
ψ	stream function [m^2 s^{-1}]
ψ'_1	net circulating flow [m^2 s^{-1}]
ω	vorticity [s^{-1}]
Ω	angular velocity [s^{-1}].

Subscript and superscripts

1	value at the inner cylinder
2	value at the outer cylinder
'	value in the rotating frame.

Other symbols

∇	gradient
$\nabla\cdot$	divergence
∇^2	Laplacian
$\nabla\times$	curl
$\times$	cross-product.

introduced a second Rayleigh number based on radial acceleration in addition to the usual gravity-based Rayleigh number. It was found that when radial acceleration dominates over gravity (strong rotation), steady-state flows are obtained in the rotating coordinate system. There is a critical Rayleigh number needed to establish the initial two-cell state and the subsequent flow patterns are multicellular. For weak rotation, the flow is bicellular and steady in the inertial coordinate system. When radial acceleration and gravity are comparable, complex time-dependent solutions result in both systems and the largest flow and heat transfer rates are found. For both weak and strong rotation, there is also an optimum Reynolds number based on the rotation speed that gives the maximum effect of gravity. It was once again confirmed that for weak rotation, if the Reynolds number becomes larger than the optimum value, the flow field approaches solid-body rotation in the inertial frame and the temperature field approaches the pure conduction state.

In the present paper, it will be shown that multiple solutions can be obtained for weak rotation and the abrupt transitions are possible between a solution involving significant buoyancy effects and a solution very near solid-body rotation, a previously unreported feature for this type of flow. The geometry being considered is an horizontal annular cavity rotating about its axis at constant angular velocity as shown in Fig. 1. Isothermal boundary conditions are prescribed at both walls, the outer being warmer. Kuehn and Goldstein [8] investigated this flow configuration in the absence of rotation. We exclude from the start high rotation speeds where the centrifugal force becomes the main body force (Bénard cells are then expected to occur beyond a critical Reynolds number, with their axes parallel to the rotation axis, e.g. Busse [9]) and concentrate on the low rotation regime, where gravity is the main body force, assuming a two-dimensional flow in the r, θ plane.

2. MATHEMATICAL FORMULATION

The problem at hand is better solved numerically in the non-inertial coordinate system rotating along with the enclosure at constant angular velocity Ω shown in Fig. 1. The analysis will then be carried out in terms of the relative flow field $\mathbf{u}'$ induced by the sole natural convection effects, that is, what would appear to an observer fixed with respect to the rotating boundaries.

The problem will be formulated with the help of the standard Boussinesq approximation, neglecting centripetal acceleration in the thermal expansion term, for a fluid of constant thermal properties. The governing equations in the rotating frame are then readily obtained from the theory of rotating flows, as exposed in Greenspan [10]. Introducing the appropriate variables

$$r^* = r/r_1 \qquad (u', v')^* = (u', v')r_1/\alpha$$
$$t^* = \alpha t/r_1^2 \qquad p^* = p_d r_1^2/\rho_1\alpha^2$$
$$\omega^* = r_1^2\omega/\alpha \qquad \psi^* = \psi/\alpha$$
$$T^* = (T-T_1)/(T_2-T_1)$$

where $p_d = p - \rho_1 \mathbf{g}'\cdot\mathbf{r}' - \rho_1\Omega^2 r^2/2$ stands for the dynamic pressure. Dropping the asterisks from now on, the problem can be stated as follows

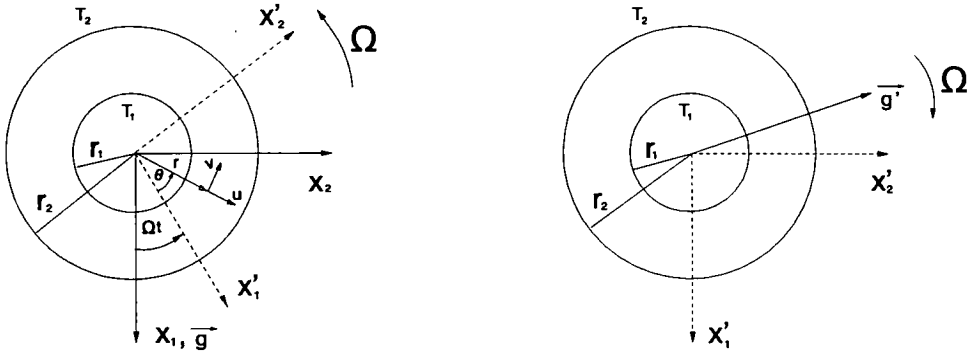

inertial frame rotating frame

FIG. 1. Geometry and coordinate system.

$$\nabla \cdot \mathbf{u}' = 0 \tag{1}$$

$$\frac{D\mathbf{u}'}{Dt} + 2Re\,Pr\,\hat{\mathbf{z}} \times \mathbf{u}' = -\nabla p + Pr\,\nabla^2 \mathbf{u}' - Pr\,Ra\,T\hat{\mathbf{g}}' \tag{2}$$

$$\frac{DT}{Dt} = \nabla^2 T. \tag{3}$$

In the momentum equation (2), $Ra = \beta(T_2 - T_1) \times r_1^3 g/\nu\alpha$ is the Rayleigh number based on gravity, and $Re = \Omega r_1^2/\nu$ is the rotational Reynolds number. In a more general formulation which does not neglect the centripetal acceleration in the Boussinesq term, an additional Rayleigh number $Ra_\Omega = \beta(T_2 - T_1) \times r_1^4\Omega^2/\nu\alpha$ would appear on the right-hand side. However, only weak rotations are considered, namely $Ra_\Omega \ll Ra$. This simplification will lead to steady/time-periodic streamline patterns in the inertial/rotating frame and is only mildly restrictive. As a matter of fact, a quick calculation for water at room temperature, considering a 5 cm gap between the cylinders, shows that Ra_Ω is still three orders of magnitude smaller than Ra when $Re = 1000$.

The temperature field satisfies the Dirichlet boundary conditions

$$T = 0; \quad r = 1 \tag{4}$$

$$T = 1; \quad r = R \tag{5}$$

and the velocity field vector components obey the usual no-slip conditions. The pressure gradient and the Coriolis force are eliminated at once by taking the curl of (2), which yields the equation

$$\frac{D\omega'}{Dt} = Pr\,\nabla^2\omega' - Pr\,Ra\,\nabla \times T\hat{\mathbf{g}}' \tag{6}$$

for the dimensionless relative vorticity

$$\omega' = \frac{1}{r}\frac{\partial rv'}{\partial r} - \frac{1}{r}\frac{\partial u'}{\partial \theta}. \tag{7}$$

Velocity components and vorticity itself may be expressed in terms of the relative stream function ψ' as

$$u' = \frac{1}{r}\frac{\partial \psi'}{\partial \theta} \tag{8}$$

$$v' = -\frac{\partial \psi'}{\partial r} \tag{9}$$

$$\omega' = -\nabla^2 \psi' \tag{10}$$

and the continuity equation (1) is then identically satisfied. It is appropriate here to point out that the relative velocities, vorticity and stream function in the rotating frame are simply related to their inertial counterparts by

$$\mathbf{u} = \mathbf{u}' + Re\,Pr\,\hat{\mathbf{z}} \times \mathbf{r}' \tag{11}$$

$$\omega = \omega' + 2Re\,Pr \tag{12}$$

$$\psi = \psi' + \frac{Re\,Pr}{2}(R^2 - r^2) \tag{13}$$

while the components of a general vector $\mathbf{f}$ transform according to

$$\begin{Bmatrix} f_r' \\ f_\theta' \end{Bmatrix} = \begin{bmatrix} \cos(\varphi) & \sin(\varphi) \\ -\sin(\varphi) & \cos(\varphi) \end{bmatrix} \begin{Bmatrix} f_1 \\ f_2 \end{Bmatrix} \tag{14}$$

where

$$\varphi = Re\,Pr\,t + \theta. \tag{15}$$

Thus, for instance, the components of the unit vector $\hat{\mathbf{g}}'$ are obtained by setting $\hat{g}_1 = 1$ and $\hat{g}_2 = 0$, respectively. Using the latter, the curl appearing in (6) can be expressed in the local r, θ coordinates of the non-inertial frame, giving the vorticity equation in its final form

$$\frac{D\omega'}{Dt} = Pr\,\nabla^2\omega' + Pr\,Ra\left\{\frac{\partial T}{\partial r}\sin(\varphi) + \frac{\cos(\varphi)}{r}\frac{\partial T}{\partial \theta}\right\}. \tag{16}$$

Moreover, periodicity of the solution in the rotating frame requires that all field variables be functions of (r, φ) only. It is possible therefore to get a formulation

in terms of $T(r, \varphi)$ and $\psi'(r, \varphi)$ which is better suited for perturbation methods. Combining (10) and (16) and changing variables gives

$$\nabla^4\psi' = Re\frac{\partial\nabla^2\psi'}{\partial\varphi} + \frac{1}{r\,Pr}\left\{\frac{\partial\psi'}{\partial\varphi}\frac{\partial\nabla^2\psi'}{\partial r} - \frac{\partial\psi'}{\partial r}\frac{\partial\nabla^2\psi'}{\partial\varphi}\right\} + Ra\left\{\frac{\partial T}{\partial r}\sin(\varphi) + \frac{\cos(\varphi)}{r}\frac{\partial T}{\partial\varphi}\right\} \quad (17)$$

$$\nabla^2 T = Re\,Pr\frac{\partial T}{\partial\varphi} + \frac{1}{r}\left\{\frac{\partial\psi'}{\partial\varphi}\frac{\partial T}{\partial r} - \frac{\partial\psi'}{\partial r}\frac{\partial T}{\partial\varphi}\right\}. \quad (18)$$

The value of ψ' may be arbitrarily fixed on only one of the boundaries. Assuming that

$$\psi' = \psi'_1; \quad r = 1 \quad (19)$$

$$\psi' = 0; \quad r = R \quad (20)$$

where ψ'_1 corresponds to the relative flow rate around the annulus whose value has yet to be determined. Two additional boundary conditions follow from the no-slip condition at the walls, namely

$$\frac{\partial\psi'}{\partial r} = 0; \quad r = 1, R. \quad (21)$$

A fourth condition may be obtained by taking advantage of the constant wall temperatures. Integrating (2) around the outer boundary yields

$$\int_0^{2\pi}\nabla^2\frac{\partial\psi'}{\partial r}\bigg|_{r=R}\mathrm{d}\theta = 0. \quad (22)$$

3. METHODS OF SOLUTION

3.1. *Numerical solution*

Solutions for the temperature and relative flow fields may be obtained by standard finite-difference methods. The governing equations (3) and (16) for temperature and vorticity are solved with the help of the alternating direction implicit method (ADI). A successive overrelaxation method (SOR) is used to solve the Poisson equation (10) for the stream function. All derivatives are discretized according to the usual Taylor-based, second order central difference scheme for a regular mesh size. Computations are carried out at each time step, using the latest available field values to get the new T, ψ', ω' values and making only one field sweep per step to calculate T and ω'.

Periodic boundary conditions are used in the θ-direction for all variables. Although (10) could in theory be used to provide boundary values for vorticity at $r = 1$ and $r = R$, it turns out to be more practical, from a numerical point of view, to obtain them as follows. Performing a power series expansion in Δr of the stream function at, say $r = R$, expressing next the derivatives of ψ at $r = R$ in terms of ω from (10) and using the no-slip condition yields

$$\psi(R-\Delta r,\theta) = \psi - \omega\frac{\Delta r^2}{2} + \left(\frac{\partial\omega}{\partial r} - \frac{\omega}{r}\right)\frac{\Delta r^3}{6} \quad (23)$$

correct to third order, where the right-hand side is evaluated at $r = R$. The remaining derivative is then discretized and the equation solved for ω at the wall in terms of quantities known from the last iteration.

When the ψ' equation is being solved, the value at the inner wall is not known explicitly, but only implicitly through the set of boundary conditions (19)–(22). In order to find the right value, an alternative approach is used which does not require the integral relation (22). Integrating $\mathbf{r}\times\mathrm{D}\mathbf{u}'/\mathrm{D}t$ over the annulus, using periodicity, leads after a few simplifications to

$$\int_1^R\int_0^{2\pi} r^2\left\{\frac{\partial^2\psi'}{\partial r\,\partial t} + Ra\,Pr\,T\sin(\varphi)\right\}\mathrm{d}r\,\mathrm{d}\theta = Pr\int_0^{2\pi}\left[r^2\frac{\partial^2\psi'}{\partial^2 r}\right]_{r=1}^{r=R}\mathrm{d}\theta \quad (24)$$

which expresses the torque equilibrium, with respect to the geometric center of the cavity, between the inertial, gravitational and viscous forces in the rotating frame. The value of ψ'_1 can be adjusted once equation (10) has been solved so that the above is satisfied. The correction can be made just once every time step as mentioned by Prud'homme *et al.* [11]. The accuracy of the numerical calculations was checked by repeating the computations of Kuehn and Goldstein [8] for a non rotating annulus. The results for the Nusselt number at $Ra = 24\,212$ for $R = 2.6$ and $Pr = 5$ agreed within 1.5–2%. All the present calculations with the rotating annulus were done with a time step $\Delta t = 0.0005$, after testing with $\Delta t = 0.0002$ showed that the larger step could be used without affecting the results. A grid dependence test was further made at $Ra = 20\,000$ which revealed that using a 27 by 54 instead of an 18 by 36 uniform mesh barely changed the predicted average Nusselt number and extremum values of ψ and produced virtually identical streamline and isotherm patterns.

3.2. *Perturbation solution*

One of the first features to be considered in a system rotating about a horizontal axis is the effect of incipient rotation combined with free convection, which locks a large mass of the fluid in the cavity to the gravity vector. How a weak rotation rate affects the symmetry of the two convection cells that are found when no rotation is present can be understood analytically. We will now show that ψ'_1 is, to the leading order, proportional to $Ra^2\,Re$. The system (17), (18) together with the boundary conditions (4), (5) for T and (19)–(22) for ψ' defines a regular perturbation problem. Expanding the field variables as

$$\psi'(r,\varphi) = \sum_{n=0}^{\infty} Ra^n\phi_n \quad (25)$$

$$T(r,\varphi)=\sum_{n=0}^{\infty} Ra^n T_n \tag{26}$$

and substituting into the governing equations yields for $n \geqslant 1$ the sequence

$$\nabla^4\phi_n = Re\frac{\partial\nabla^2\phi_n}{\partial\varphi} + \frac{1}{r\,Pr}\sum_{i=0}^{i=n}\left\{\frac{\partial\phi_i}{\partial\varphi}\frac{\partial\nabla^2\phi_{n-i}}{\partial r}-\frac{\partial\phi_i}{\partial r}\frac{\partial\nabla^2\phi_{n-i}}{\partial\varphi}\right\} + \frac{\partial T_{n-1}}{\partial r}\sin(\varphi)+\frac{\cos(\varphi)}{r}\frac{\partial T_{n-1}}{\partial\varphi} \tag{27}$$

$$\nabla^2 T_n = Re\,Pr\frac{\partial T_n}{\partial\varphi}+\frac{1}{r}\sum_{i=0}^{i=n}\left\{\frac{\partial\phi_i}{\partial\varphi}\frac{\partial T_{n-i}}{\partial r}-\frac{\partial\phi_i}{\partial r}\frac{\partial T_{n-i}}{\partial\varphi}\right\} \tag{28}$$

where each ϕ_n must satisfy the original boundary conditions (19)–(22) and each T_n the homogeneous Dirichlet conditions. The zeroth-order solution gives the pure conduction state, that is, $\phi_0 = 0$ and

$$T_0 = \ln(r)/\ln R. \tag{29}$$

The first-order equations read

$$\nabla^4\phi_1 = Re\frac{\partial\nabla^2\phi_1}{\partial\varphi}+\frac{1}{\ln R}\frac{\sin(\varphi)}{r} \tag{30}$$

$$\nabla^2 T_1 = Re\,Pr\frac{\partial T_1}{\partial\varphi}+\frac{1}{r^2\ln R}\frac{\partial\phi_1}{\partial\varphi}. \tag{31}$$

A solution of (30) is readily found by separation of variables in terms of the Bessel functions of order one, giving ϕ_1 as twice the real part of

$$\left\{a_1^1 r + a_2^1 r^{-1} + a_3^1 J_1(i^{3/2}Re^{1/2}r) + a_4^1 K_1(i^{1/2}Re^{1/2}r) + \frac{r\ln(r)}{4Re\ln R}\right\}e^{i\varphi} \tag{32}$$

where $a_1^1, a_2^1, a_3^1, a_4^1$ are complex coefficients to be determined from the boundary conditions. In the above expression, J_1 is the Bessel function of the first kind, and K_1 is the modified Bessel function of the second kind. The real and imaginary parts of J_1, K_1 are also known as the Kelvin functions of order one. In any case, with all the radial terms in (32) multiplied by either $\sin(\varphi)$ or $\cos(\varphi)$, the integral condition (22) becomes redundant, and the entire inner wall can be a streamline if ϕ_1 is locally zero there. The values of the four unknown coefficients are then found by requiring that ϕ_1 and its first derivative with respect to r vanish at both walls.

Thus ϕ_1 has no contribution to ψ'_1 and we need to seek higher-order terms in the expansion (25). Solving next for T_1 is an awkward task because the right-hand side of (31) now involves the complex Bessel (or Kelvin) functions. But since we are interested in only the initial effects of rotation, it is more convenient (and considerably simpler) to proceed with a second expansion of the form $\phi_1 = f_0 + Re\,f_1 + \ldots$ in (30) and $T_1 = g_0 + Re\,g_1 + \ldots$ in (31) than to try to solve the set of equations for arbitrary Reynolds numbers. The second expansion gives

$$\nabla^4 f_0 = \frac{1}{\ln R}\frac{\sin(\varphi)}{r} \tag{33}$$

$$\nabla^4 f_1 = \frac{\partial\nabla^2 f_0}{\partial\varphi} \tag{34}$$

$$\nabla^2 g_0 = \frac{1}{r^2\ln R}\frac{\partial f_0}{\partial\varphi} \tag{35}$$

$$\nabla^2 g_1 = Pr\frac{\partial g_0}{\partial\varphi}+\frac{1}{r^2\ln R}\frac{\partial f_1}{\partial\varphi}. \tag{36}$$

Solution can be achieved by separation of variables as before, giving f_0, f_1, g_0, g_1 as linear combinations of terms of the form $r^u \ln^h(r)$ multiplied by either $\sin(\varphi)$ or $\cos(\varphi)$. Writing out (27) in full for $n = 2$, an expansion $\phi_2 = h_0 + Re\,h_1 + \ldots$, done along the same lines, shows that at any order in Re, all the terms in h_0 will also exhibit a similar angular dependence and, again, vanish at $r = 1$. On the other hand, h_1 contains terms which are independent of φ and therefore do not necessarily vanish at $r = 1$, giving

$$\psi'_1 = C\,Ra^2\,Re + \ldots \tag{37}$$

in the first approximation, where $C(R, Pr)$ is an intricate algebraic expression involving R, $\ln R$, Pr. Values of the coefficient C are given in Table 1 for several radii ratios and Prandtl numbers.

Table 1. Value of C in (37) vs Pr and R

	$Pr = 0.7$	$Pr = 1$	$Pr = 7$
$R = 1.5$	-1.070×10^{-9}	-1.413×10^{-9}	-8.260×10^{-9}
$R = 2.0$	-4.185×10^{-7}	-5.518×10^{-7}	-3.210×10^{-6}
$R = 2.5$	-1.255×10^{-5}	-1.652×10^{-5}	-9.558×10^{-5}
$R = 3.0$	-1.336×10^{-4}	-1.754×10^{-4}	-1.010×10^{-3}
$R = 3.5$	-8.125×10^{-4}	-1.065×10^{-3}	-6.098×10^{-3}
$R = 4.0$	-3.487×10^{-3}	-4.561×10^{-3}	-2.601×10^{-2}

4. RESULTS

All calculations were performed for a Prandtl number $Pr = 1$ using the 18 by 36 uniform mesh, unless stated otherwise. Results are presented below versus Re at different Rayleigh numbers ranging from $Ra = 0$ to $Ra = 10^5$.

Typical streamline and isotherms obtained with the 27 by 54 mesh for $Ra = 10^4$ are depicted in Fig. 2, for a cavity aspect ratio $R = 2$, in both inertial and non-inertial frames. From left to right are shown the patterns corresponding to ψ', T and ψ respectively. Clockwise rotation is assumed throughout in the inertial frame, where the ψ stream function is steady. The relative flow field is therefore time-periodic, with the ψ' streamlines rotating along with the gravity vector

in the counterclockwise direction. For convenience, both flows are represented with the gravity vector pointing downwards. The isotherms are, for course, identical in both frames. It is obvious from the figure that the original symmetry with respect to a vertical diameter, found when there is no rotation, disappears quickly as Re increases and a net circulating flow ψ'_1 is established around the annulus, as predicted by the perturbation analysis. The latter increases steadily with Re until a critical value Re_{cr} is reached for which a bifurcation occurs which sets apart two distinct regimes of flow behavior, illustrated by the streamline patterns of Figs. 2(d) and 2(e) respectively.

4.1. *The shear and solid-body rotation regimes*

It is clear from the figure that Re_{cr} lies between 74 and 75 for this Rayleigh number. Before the bifurcation occurs, a significant mass of fluid in the annular gap does not take part in the rotation but remains essentially tied up to gravity. This gives rise to large velocity gradients near the boundaries, as shown by the streamlines in the inertial frame, like in Fig. 2(d),

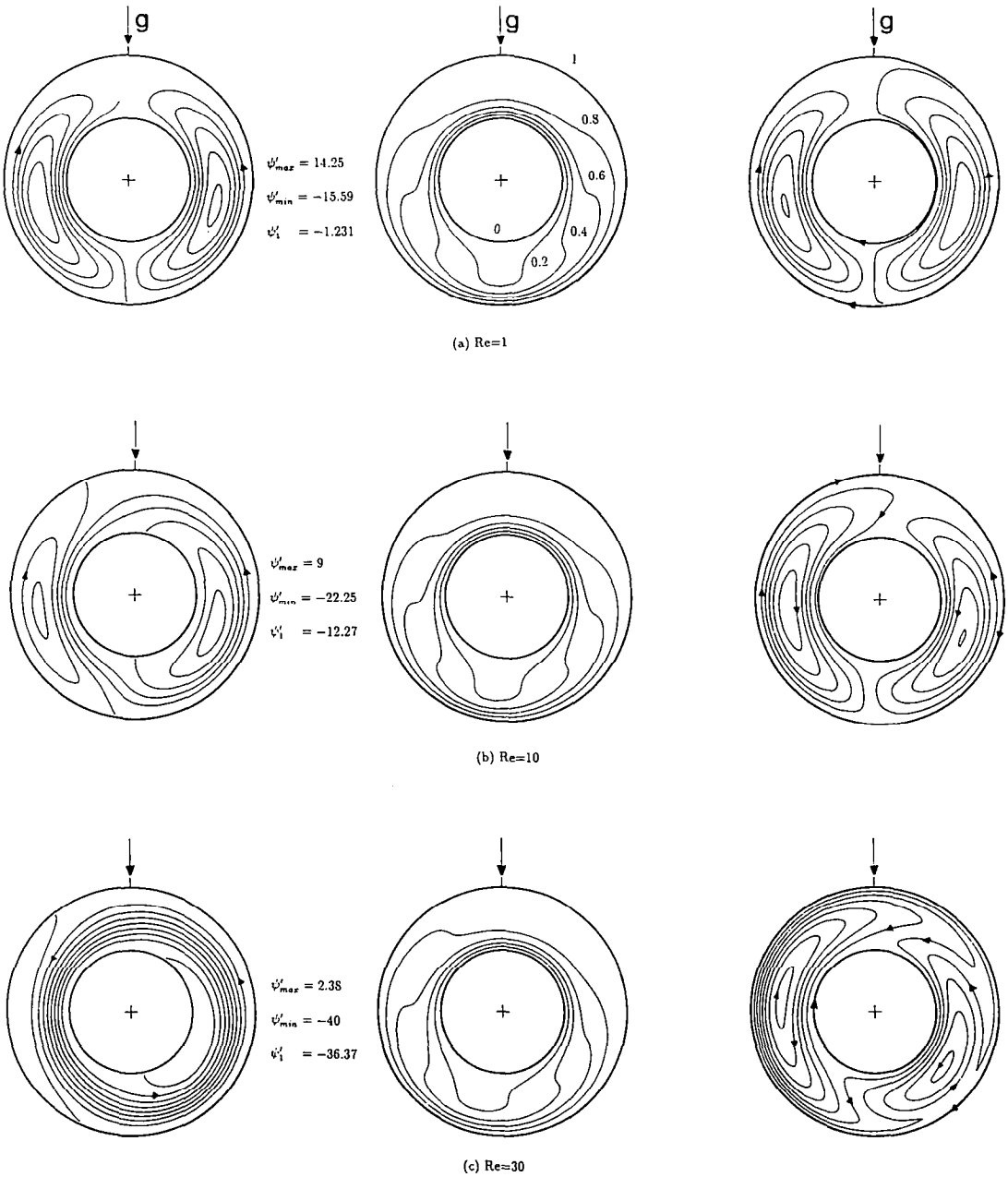

FIG. 2. Streamlines and isotherms, $Ra = 10000$, $R = 2$. The ψ' streamlines (left column) are rotating counterclockwise. The ψ streamline graphs (right column) represent steady-state flows with boundaries rotating clockwise.

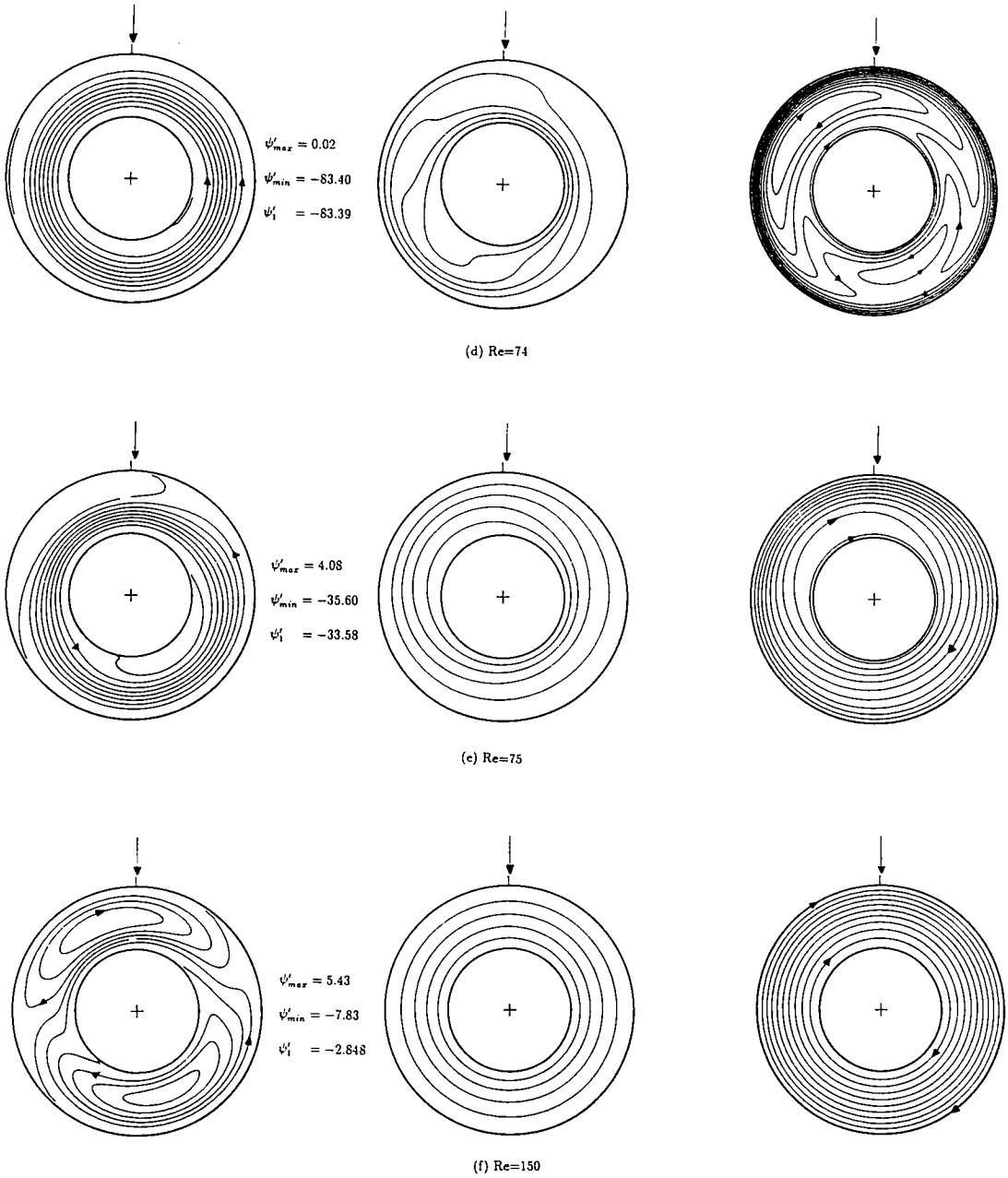

FIG. 2.—*Continued.*

for instance. A relatively important torque is consequently imposed on the fluid through boundary shear forces, as depicted in Fig. 3. This torque is balanced by a countertorque due to gravity forces on the fluid of non-homogeneous density. The magnitude of this gravitational torque is closely related to the degree of asymmetry of the temperature field with respect to a vertical diameter. The increasing distortion of the isotherms maintains the equilibrium between the torques up to $Re = 74$. The range $0 < Re < Re_{cr}$, characterized by an intense relative circulation ψ'_1 around the annulus, accompanied by high levels of shear stress at the boundaries, could be called the shear regime therefore.

The solid-body rotation regime takes place when Re exceeds the critical Re_{cr} value. When this happens, ψ'_1 is drastically reduced and the shear flow regime cannot be sustained anymore. We notice a drastic change in the steamline and isotherm patterns between Figs. 2(d) and 2(e), showing a very different type of flow behavior. The paths of the fluid particles become almost circular in the inertial frame, and a new equilibrium prevails between the shear and gravitational forces, which implies a much lower level of shear

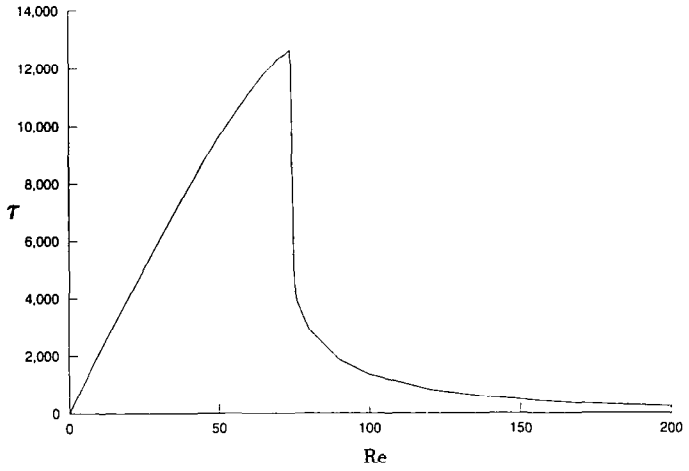

FIG. 3. Net shear torque on the fluid vs Re, $Ra = 10000$, $R = 2$.

torque, as revealed by Fig. 3. As Re is increased further above 75, ψ'_1 decreases asymptotically toward zero and the nearly pure solid-body rotation flow of Fig. 2(f) is achieved.

Figure 4 shows the relative flow rate ψ'_1 circulating around the annulus versus Re for $R = 2$ and Ra up to 10^5. The inclined straight dashed line represents the limiting case of an inviscid fluid slipping at the walls.

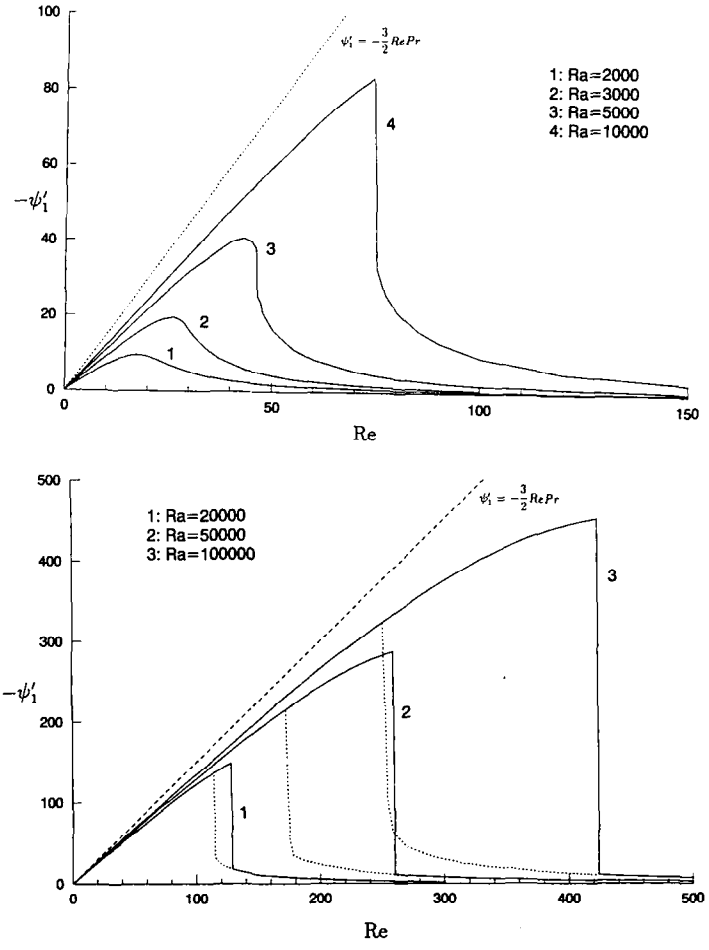

FIG. 4. Relative flow rate around the annulus vs Re, $R = 2$.

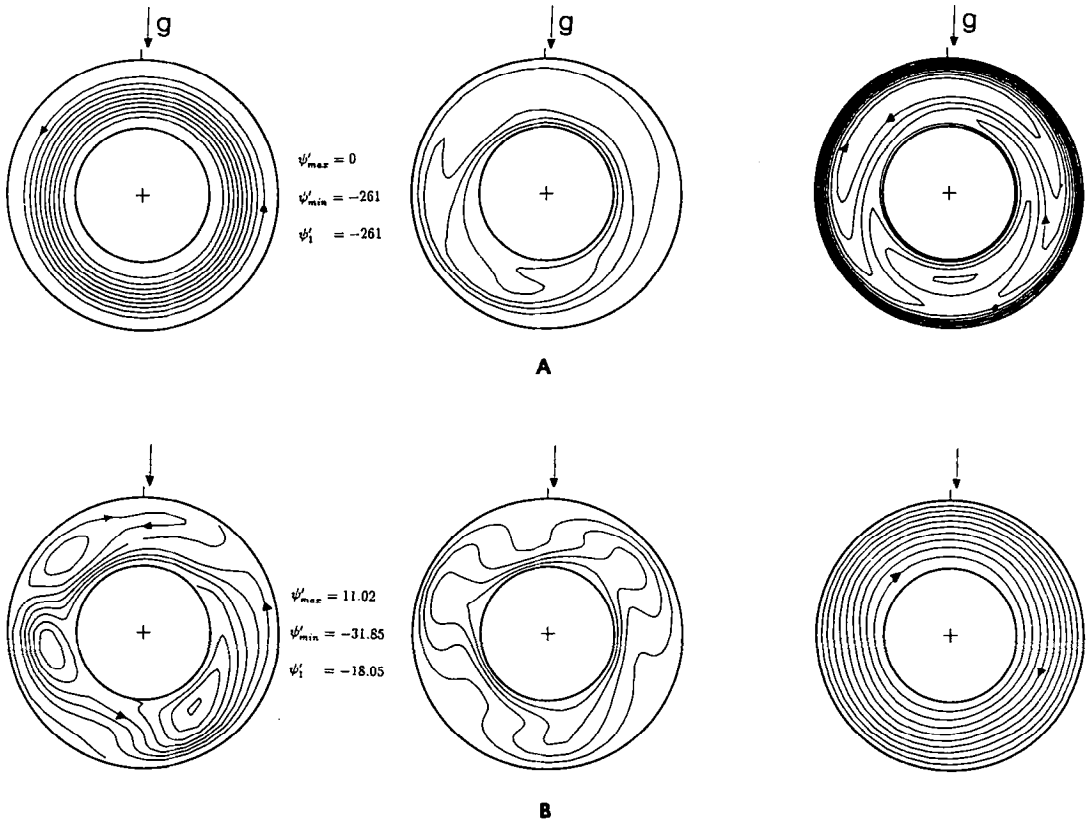

FIG. 5. Hysteresis effect, $Ra = 50\,000$, $Re = 220$, $R = 2$: (a) shear-flow regime; (b) solid-body rotation regime.

In this hypothetical situation, there would be no net circulation in the inertial frame whatsoever. Setting therefore $\psi = 0$ at $r = 1$ in (13) gives

$$-\frac{\partial \psi'_i}{\partial Re} = \frac{Pr}{2}(R^2 - 1) \tag{38}$$

as the initial slope for an inviscid fluid. The curves shown in Fig. 4 exhibit slopes almost as steep when $Re \to 0$, and subsequently depart from the inviscid asymptote as Re increases. For an actual (i.e. viscous) fluid however, boundary layers are formed at the walls. This implies that without buoyancy effects, the whole mass of fluid is eventually entrained by momentum diffusion from the walls into a steady-state, solid-body rotation. Thus, $\psi'_i = 0$ when $Ra = 0$.

The plots corresponding to the lower values of Ra show a progressive transition between the flow regimes as the circulation increases, goes through a

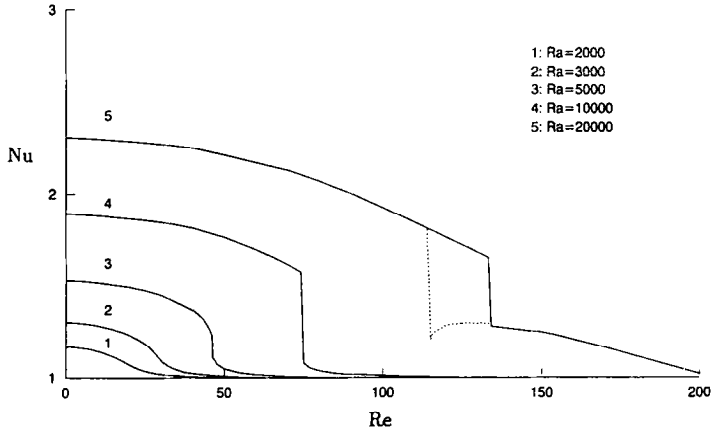

FIG. 6. Average Nusselt number at inner boundary vs Re, $R = 2$.

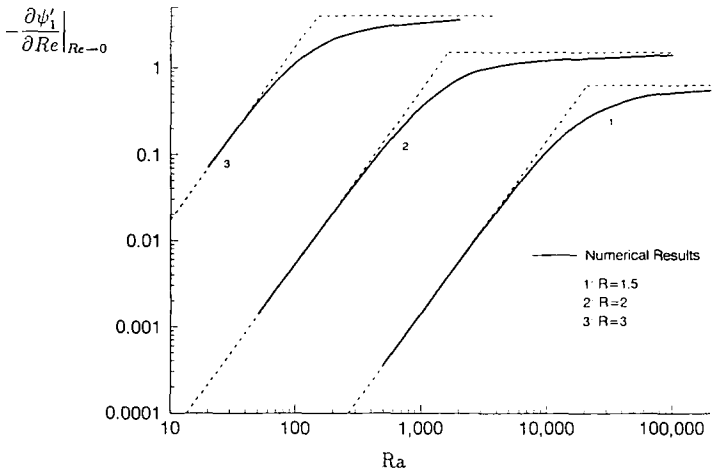

FIG. 7. Onset of the relative flow rate ψ_1' around the annulus: Solid line: numerical results; Inclined dashed lines: perturbation solution (37); Horizontal dashed lines: inviscid asymptote (38).

maximum and decreases. These trends are similar so far to those reported by Robillard and Torrance [6] in the case of an annular rotating porous layer. Unlike in the porous case, however, the present results show that a discontinuity in the ψ' profiles gradually builds up with Ra which sets apart the two regimes illustrated by the streamline patterns of Figs. 2(d) and 2(e) respectively. For $Ra > 5 \times 10^3$, the smooth transition is replaced by the bifurcation discussed earlier, which always occurs when σ is of order one, that is, when rotation effects become strong enough to overcome buoyancy. This type of flow behavior was not observed in the rotating porous medium. For the latter, fluid entrainment is done locally throughout the annulus by the bulk rotation of the porous matrix, not by viscous diffusion from the boundaries. Consequently, it is impossible in the porous case for ψ_1' to maintain its initial slope as Re increases. Going back to Fig. 4, a definite hysteresis effect is displayed at $Ra = 2 \times 10^4$ and above, allowing both solution regimes over a certain range of Reynolds numbers. The upper branch (solid curves), for increasing Reynolds numbers, may be obtained step by step, using the previous result at a lower Re as the initial condition for the next computation until transition occurs. The procedure is then reversed to get the lower branch (dashed curves), starting from the solid-body regime and decreasing Re. The critical values are sharply defined for both solution branches. Transition occurs perhaps within an interval of less than one percent of Re_{cr}, which is also not very sensitive to grid refinement. However, subsequent testing revealed that R appears to be an influential parameter on hysteresis, as could be expected. For instance, increasing R reduces the range of Re over which both regimes are possible. Further investigation would be needed in order to obtain a complete description of the effects of this parameter. Figure 5 shows the two solutions that can be obtained for $Ra = 5 \times 10^4$ and $R = 2$ in the region of overlap, at $Re = 220$. The difference in character is obvious from the ψ patterns on the right.

Average Nusselt numbers at the inner boundary, normalized by the value for pure conduction, defined as

$$Nu = \frac{\ln R}{2\pi} \int_0^{2\pi} \frac{\partial T}{\partial r}\Big|_{r=1} d\theta \qquad (39)$$

are shown in Fig. 6. The plots of Nu exhibit the same sharp transitions and hysteresis effects when Ra is high enough as the ψ' profiles. However, some oscillations of Nu were found to occur on the lower branch of solution when hysteresis was present, and that for all grids and time steps used. So the dashed curve for $Ra = 20\,000$ has indicative value only. Initially, all the Nu profiles remain well above unity since the convective flow of the shear regime favors heat exchange between the boundaries. Convective heat transfer efficiency is directly related to the amplitude of the radial motion of the fluid particles, which remains important throughout the shear regime, as can be inferred from the steady ψ streamline patterns of Figs. 2(a)–(d). On the other hand, all profiles decrease toward the pure conduction unity value in the solid-body rotation regime.

4.2. *The onset of circulation as* $Re \to 0$

The initial effects of rotation on the convective flow were investigated numerically for several radii ratios of the cavity in order to assess the range of validity of (37). An interesting comparison between the analytical and numerical results is provided in Fig. 7, where the inclined and horizontal dashed lines represent the analytical solutions (37) for incipient convection and the inviscid asymptotes given by (38), respectively. Taking $R = 2$, that is, inner cavity radius equal to the annular gap, the agreement appears to be excellent up to Ra around 500. Departure from the

quadratic profiles (37) occurs with increasing Ra and the numerical results subsequently show a tendency to level out below the inviscid asymptotes, as expected.

5. CONCLUSION

Analytical and numerical calculations were carried out to study mixed convection in a fluid filled annular region with boundaries rotating at the same angular velocity. Two flow regimes were distinguished: shear flow and solid-body rotation. The former is characterized by the existence of a large fluid core tied up to gravity, which does not take part in the rotation around the cavity imposed by the solid boundaries. As a consequence, a significant flow rate is created around the annulus with respect to a reference frame rotating with the boundaries. The onset of this flow has been shown analytically to be dependent upon the square of the Rayleigh number. Bifurcation is possible if the Rayleigh number is high enough, after which the shear regime ceases abruptly while the whole mass of fluid undergoes solid-body rotation and the heat transfer process reverts to pure conduction. At higher Rayleigh numbers hysteresis effects are evidenced, with both regimes overlapping within a given range of Reynolds numbers.

Acknowledgement—This research was supported by the Natural Sciences and Engineering Research Council of Canada.

REFERENCES

1. H. Q. Yang, K. T. Yang and J. R. Lloyd, Rotational effects on natural convection in a horizontal cylinder, *A.I.Ch.E. Jl* **34**, 1627–1633 (1988).
2. L. E. Clifcorn, G. T. Peterson, J. M. Boyd and J. H. O'Neil, A new principle for agitating in processing of canned foods, *Fd. Technol.* **4**, 450–460 (1950).
3. F. Ladeinde, Studies of thermal convection in self-gravitating and rotating horizontal cylinders in a vertical external gravity field, Ph.D. Thesis, Cornell University, Ithaca, New York (1988).
4. T. S. Lee, Numerical experiments with laminar fluid convection between concentric and excentric heated rotating cylinders, *Num. Heat Transfer* **7**, 77–87 (1984).
5. T. Fusegi, B. Farouk and K. S. Ball, Mixed convection flows within a horizontal concentric annulus with a heated rotating inner cylinder, *Num. Heat Transfer* **9**, 591–604 (1986).
6. L. Robillard and K. E. Torrance, Convective heat transfer in an annular porous layer rotating at weak angular velocity, *Int. J. Heat Mass Transfer* **33**, 953–963 (1990).
7. F. Ladeinde and K. E. Torrance, Convection in a rotating, horizontal cylinder with radial and normal gravity forces, *J. Fluid Mech.* **228**, 361–385 (1991).
8. T. H. Kuehn and R. J. Goldstein, An experimental and theoretical study of natural convection in the annulus between horizontal cylinders, *J. Fluid Mech.* **74**, 695–719 (1976).
9. F. H. Busse, Asymptotic theory of convection in a rotating cylindrical annulus, *J. Fluid Mech.* **173**, 545–556 (1986).
10. H. P. Greenspan, *The Theory of Rotating Fluids*. Cambridge University Press, (1969).
11. M. Prud'homme, L. Robillard and P. Vasseur, A study of laminar natural convection in a non-uniformly heated annular fluid layer, *Int. J. Heat Mass Transfer* **30**, 1209–1222 (1987).